Understanding doping effects in biosensing using carbon nanotube network field-effect transistors

Jiantong Li and Shi-Li Zhang*
School of Information and Communication Technology, Royal Institute of Technology (KTH), Electrum 229, SE-164 40 Kista, Sweden
(Received 24 October 2008; published 22 April 2009)

Systematic theoretical studies based on a comprehensive heterogeneous stick percolation model are performed to gain insights into the essence of doping effects in electrical sensing of biomolecules, such as proteins and DNA fragments, using carbon nanotube network field-effect transistors (CNNFETs). The present work demonstrates that the electrical response to doping of CNNFETs is primarily caused by conductance change at the electrode-nanotube contacts, in contrast to that in the channel as assumed previously. However, the presence of intertube junctions in the channel could reduce the sensitivity of CNNFET-based biosensors and is partially responsible for the experimentally observed channel-length dependent sensitivity.

DOI: 10.1103/PhysRevB.79.155434 PACS number(s): 85.35.Kt, 73.63.Fg

I. INTRODUCTION

Carbon nanotube network field-effect transistors (CNNFETs) (Ref. 1) have recently been intensively studied for a variety of potential applications including flexible electronics, solar cells, and sensors.[2–4] Building a CNNFET is relatively straightforward since it avoids the extremely demanding proposition, as is indispensable for devices based on individual single-walled carbon nanotubes (SWCNTs),[3–5] to control the property, position and/or orientation of individual SWCNTs. High-yield production of CNNFETs is hence viable. As for applications in sensing biomolecules, such as proteins and DNA fragments, specific superiority of CNNFETs has further been proposed, including the considerable sensitivity and significant suppression of electrical $(1/f)$ noise.[6] However, some studies have also pointed out that CNNFET-based biosensors have much lower sensitivity than those based on silicon nanowire arrays[7] and no exclusive mechanism can be concluded as responsible for the sensing. Typically, two major sensing mechanisms have been proposed to account for the detected conductance variations in response to the introduction of biomolecules.[6–12] One is electron doping resulting from adsorption of the molecules on the SWCNTs, which has been correlated with fluorescence studies.[6,8] The other is the modification of metal work function of the electrodes, which may be supported by experimental observations that the responsible region for sensing (conductance change) is the vicinity of electrode-SWCNT contacts, not the channel.[9,11] In some studies,[8] the former is further categorized as channel-dominated mechanism since doping is assumed to change the conductance of SWCNTs in the channel, whereas the latter is contact-dominated mechanism. Motivated by the experimental evidence[6,9] for the adsorption of protein and DNA on SWCNTs and in the light of the various mechanisms discussed in the literature, we focus on establishing a general understanding of the essence of the doping-induced conductance change in CNNFET-based biosensors and investigate the responsible factors for their reduced sensitivity.

II. COMPUTATIONAL METHOD

A. Development of stick percolation model

In the literature,[2,4,13–19] the electrical characteristics of CNNFETs are usually studied theoretically based on heterogeneous stick percolation models. Such models assume a CNN to be composed of percolating networks of sticks (SWCNTs), with appropriate nanotube conductivity and intertube (SWCNT-SWCNT) junction conductance obtained experimentally or theoretically.[13,15] Extensive studies have shown that these models are rather sophisticated in calculating the gate-dependent conductance of the corresponding CNNFET. However, their shortcoming in studies on biosensing mechanisms is also significant. As mentioned above, one of the most interesting issues of the CNNFET-based biosensors is whether the conductance response upon detection of biomolecules is channel dominated or contact dominated. The existing models only take into account the conductance of nanotubes and intertube junctions without any explicit consideration of the effects of electrode-SWCNT contacts. Though the nanotube conductance is in some cases taken to be the average or effective conductance of the nanotubes and the contacts based on experimental measurements, this kind of treatment is unable to discern the difference between the effects of nanotubes (channels) and those of contacts. Such a shortcoming prevents the current models from providing a sensible theoretical frame for investigation of the sensing mechanisms of CNNFET-based biosensors.

In what follows, we will start from the existing models by considering electrode-SWCNT contacts as an indispensable part of CNNFETs. By doing so, a CNNFET comprises three major components: SWCNTs, electrode-SWCNT contacts, and intertube junctions, as schematically shown in Fig. 1. Each component has an appropriate conductance. As in the previous models,[15–17] the conductance of the CNNFET is calculated by establishing equations based on Kirchoff's law at each intertube junction along the percolation paths. However, finite conductance should be included between the SWCNTs and the source-drain electrodes to account for the existence of the electrode-SWCNT contacts.

B. Doping-dependent conductance

In order to conduct a systematic investigation on the doping effects in CNNFET-based biosensors using the developed stick percolation model, it is necessary to determine the doping dependence of the conductance of all the three components of CNNFETs. However, it is demanding to acquire

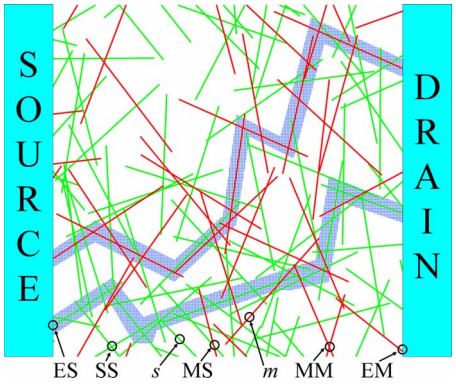

FIG. 1. (Color online) Device structure of a CNNFET used as the base for the heterogeneous stick percolation model. Each SWCNT is represented as a stick, dark gray (red for color online) for metallic (m-) SWCNT and light gray (green for color online) for semiconducting (s-) SWCNT. The nanotube network consists basically of three components: SWCNTs (m or s), electrode-SWCNT contacts (ES or EM) and intertube junctions (SS, MM, or MS). The gray hatched areas (blue hatched areas for color online) exhibit two examples of metallic (upper) and semiconducting (lower) percolation paths.

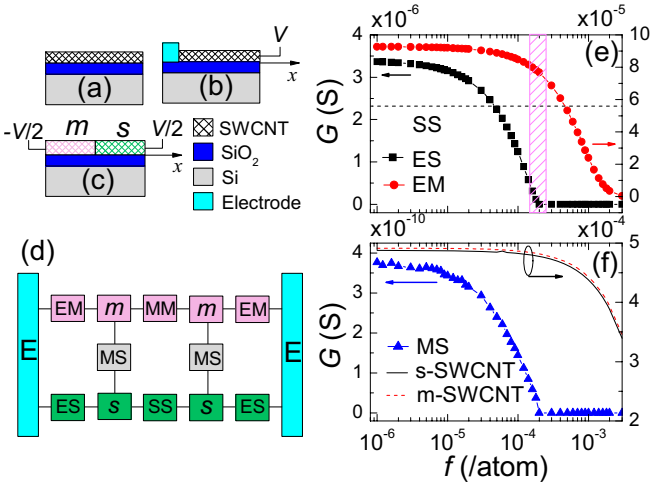

FIG. 2. (Color online) Geometries of the components in the simulated CNNFETs for (a) an SWCNT, (b) an ES/EM contact, and (c) an MS junction. (d) Equivalent circuit scheme of a typical high-density nanotube network, which consists of m-SWCNT and s-SWCNT subnetworks connecting each other by MS junctions. (e) Doping-dependent conductance (V_G=−10 V) of ES and EM contacts. ΔW=0.1 eV. The horizontal dashed line is for SS junctions with reference to the left coordinate axis. For MM junctions, the conductance is about 6×10^{-6} S, also independent of doping. Around the marked doping region, the conductance of the ES contacts is significantly suppressed while the EM contacts have weak sensitivity to doping. (f) Doping-dependent conductance (V_G=−10 V) of SWCNTs (1 μm long) and MS junctions. For conductance calculation of the ES, EM contacts, and MS junctions, the applied voltage is V=0 V and the SWCNTs are 300 nm long.

such knowledge from experiments. Before treating the CNNFET-based biosensors, the doping-dependent conductance of each component in a CNNFET is first calculated based on previously reported semiclassic models as described briefly below. Note that different from classical percolation, the SWCNT network is heterogeneous in the sense that about one-third of the nanotubes are metallic and the other two-thirds are semiconducting.[2] Therefore, for each component, both metallic SWCNTs (m-SWCNTs) and semiconducting SWCNTs (s-SWCNTs) should be considered separately; cf. Fig. 1.

1. Conductance of SWCNTs

Under low bias, the hole (p) and electron (n) concentrations in an SWCNT are related to $V_{\mathrm{NT}}(x)$, the average potential at position x along the nanotube, as[18,20]

$$p(x) = \int_{-\infty}^{0} D(E)F[eV_{\mathrm{NT}}(x) - E]dE, \tag{1a}$$

$$n(x) = \int_{0}^{+\infty} D(E)F[E - eV_{\mathrm{NT}}(x)]dE, \tag{1b}$$

where $F(E)$ is the Fermi distribution function, e is the electron charge, and $D(E)$ is the density of states (DOS) per atom.[21] Adsorbed biomolecules are suggested to generate uniformly distributed electronic doping on the SWCNT without changing its band structure.[22,23] The total charge density is found as

$$\rho(x) = eN[p(x) - n(x) + f], \tag{2}$$

where $N=\frac{4\pi d}{3\sqrt{3}a^2}$ is the atomic linear density along the SWCNT with a=0.144 nm being the carbon-carbon bonding distance, and d being the nanotube diameter, and f is the doping fraction, i.e., the number of doped charge carriers per atom of the SWCNT. The pinning effects between SWCNTs and electrodes are ignored.[24] Note that the m-SWCNTs are treated in the same manner as s-SWCNTs with regard to considering conduction carriers (holes and electrons) except that they are assigned to different DOS.[25,26]

For an SWCNT in the channel but away from the two electrodes [Fig. 2(a)], the charge density along the SWCNT is assumed to be position independent and the corresponding gate voltage is[20]

$$V_G = V_{\mathrm{NT}} - \frac{\rho}{C_{\mathrm{OX}}} + V_{\mathrm{FB}}, \tag{3}$$

where C_{OX} is the gate oxide capacitance and V_{FB} is the flat-band voltage. In this work, the effect of V_{FB} is neglected and a more accurate expression for the nonembedded cylinder-on-plate gate oxide capacitance $C_{\mathrm{OX}}=2\pi\varepsilon_0\varepsilon_{\mathrm{OX}}/\ln(4\frac{t_{\mathrm{OX}}}{d}+2)$ is used with t_{OX} as the gate oxide thickness, ε_0 the vacuum permittivity, and $\varepsilon_{\mathrm{OX}}$=2.2 the effective dielectric constant of the gate oxide.[27,28] Self-consistent calculations of Eqs. (2) and (3) generate the carrier density p and n. The conductance of SWCNTs is given by $G_p=\frac{eNp\mu_p}{L}$ and $G_n=\frac{eNn\mu_n}{L}$ for holes and electrons, respectively, with L being the length of the SWCNT or SWCNT segment. In this work, low-field mobilities $\mu_p=2.5\times10^4$ cm^2/V s and $\mu_n=2.0\times10^4$ cm^2/V s are taken from previous studies[28,29] for both s-SWCNTs and

m-SWCNTs. As the influence of carrier density on SWCNT mobility is insignificant at room temperature,[29] m-SWCNTs and s-SWCNTs are assumed to have identical mobility.

2. Conductance of electrode-SWCNT contacts

In contrast, however, the potential along the SWCNTs strongly varies with position near the electrode-SWCNT contact [Fig. 2(b)]. In this case, the potential distribution is obtained by solving the Poisson equation. For SWCNT transistors where the channel thickness (approximately the SWCNT diameter d) is much thinner than t_{OX}, the one-dimensional (1D) Poisson equation is able to describe the electrical potential along the SWCNT surface under low bias,[19,30–32]

$$\frac{d^2V_{NT}}{dx^2} - \frac{V_{NT} - V_G}{\lambda^2} = -\frac{\rho(x)}{\varepsilon_0 \varepsilon_{NT}}, \tag{4}$$

where λ is the effective screening length calculated through $\lambda^2 = \frac{d^2}{2} + \frac{\varepsilon_{NT} t_{OX} d}{\varepsilon_{OX}}$ with $\varepsilon_{NT} \approx 5$ as the dielectric constant of SWCNTs.[19,31] In Eq. (4), the hollow cylindrical structure of SWCNTs is neglected. Instead, they are treated as solid prisms. The 1D charge density $\rho(x)$ in Eq. (2) is hence averaged over its cross-sectional area d^2 to yield the equivalent three-dimensional (3D) charge density. In order to avoid short-channel effects, the SWCNT length should be sufficiently long. The boundary conditions for Eq. (4) are specified as follows. The potential at the interface is determined by $-eV_{NT}(0) = \Delta W$ where $\Delta W = W_M - W_{NT}$ is the work-function difference between the electrode metal and the SWCNT. The other end of the SWCNT is biased at the voltage of V. From self-consistent calculations of Eqs. (2) and (4), the potential distribution can be obtained and the contact conductance G_C is calculated from Landauer formula,

$$G_C = G_q \int T(E) \left(-\frac{\partial F(E)}{\partial E} \right) dE, \tag{5}$$

where $T(E)$ is the energy-dependent transmission and is evaluated based on the WKB approximation with

$$T(E) = \exp\left[-\frac{4}{3at} \int_{x_i}^{x_f} \sqrt{\Delta_0^2 - [E + eV_{NT}(x)]^2}\, dx \right] \tag{6}$$

for contacts between electrodes and s-SWCNTs (ES), and

$$T(E) = \exp\left[-\frac{4}{3at} \int_{x_i}^{x_f} |E + eV_{NT}(x)|\, dx \right] \tag{7}$$

for contacts between electrodes and m-SWCNTs (EM). Here, $t = 2.5$ eV is the tight-binding parameter, Δ_0 is the half band gap of s-SWCNTs, and x_i and x_f are classical turning points.[33–35]

3. Conductance of intertube junctions

The conductance of the junction between m-SWCNT and s-SWCNT (MS) [Fig. 2(c)] is calculated in a similar way to that of ES contacts except that for MS junctions, the work-function difference is neglected and the bias voltages at the two ends of the SWCNTs are set to $-V/2$ and $V/2$, respectively.[25,26]

However, any two SWCNTs crossing each other are actually separated by the van der Walls distance.[36] Therefore, an additional junction transmission probability T_j is included yielding the final conductance of the MS junctions as $G_{MS} = T_j G_C$. For junctions between two m-SWCNTs (MM) or two s-SWCNTs (SS), no Schottky barrier is present for identical diameter and doping of the SWCNTs.[36] The conductance is dominated by the junction transmission probability, i.e., G_{MM} (or G_{SS}) $= T_j G_q$, which should be independent of doping and gate voltage. Here $G_q = \frac{4e^2}{h}$ is two units of quantum conductance with h being Planck's constant. Based on the experimental results,[36] $T_j = 0.04$ is found for MM and MS junctions and $T_j = 0.015$ for SS junctions. Note that finite separation is also proposed to exist at the electrode-SWCNT (ES or EM) contacts,[37] especially for the side-contacted structure, due to some experimental observations of very low conductance for metal-SWCNT contacts. However, depending on their contact conditions, metal-SWCNT contacts are not always of low conductance[38] and we only consider CNNFETs with high contact conductance and high nanotube density for the sake of low $1/f$ noise.[39] Consequently, $T_j = 1$ is assumed for ES and EM contacts in this work.

III. RESULTS AND DISCUSSION

The conductance defined above for all the components forms the basis for evaluation of the conductance response of CNNFETs. In this work, we focus on the room-temperature ($T = 300$ K) electrical characteristics in linear-response region (i.e., low-bias assumption[19]) of back-gate CNNFETs with a 100-nm-thick SiO_2 layer as the gate insulator. All CNNFETs are assumed to be near equilibrium. SWCNTs of diameter $d = 1.1$ nm and length $L_S = 2$ μm are randomly generated by Monte Carlo procedure[13,16,17] to form 5-μm-wide networks as the channels of CNNFETs.

A. Responsible region

The equivalent circuit scheme of a simple but typical nanotube network, for example, that in Fig. 1, is shown in Fig. 2(d) illustrating the function of SWCNTs, contacts and junctions in CNNFETs. In our simulation, the effects of the ES and EM contacts at the drain electrode are neglected as long-channel devices are dealt with.[35] Usually, CNNFETs exhibit unipolar p-type behavior and the sensing is based on the hole conductance change at the ON state, the state on which the present work will focus. Figures 2(e) and 2(f) show the doping dependences of the calculated ON-state ($V_G = -10$ V) conductance for all the contacts, junctions and SWCNTs in a CNNFET. Their conductance sequence is m-SWCNT (1 μm long) $\approx$ s-SWCNT (1 μm long) $>$ EM $>$ ES $\approx$ MM $\approx$ SS $\gg$ MS. As seen, the ES contacts and MS junctions are sensitive to doping level as low as $f < 10^{-4}$, while the EM contacts and SWCNTs are only sensitive to high-doping level of $f > 10^{-4}$. Referred to Fig. 2(d), since both m-SWCNT and s-SWCNT have much higher conductance but lower doping sensitivity for $f < 10^{-3}$, they should play a negligible role in the conductance change in CNNFETs induced by doping. Though the MS junctions are sen-

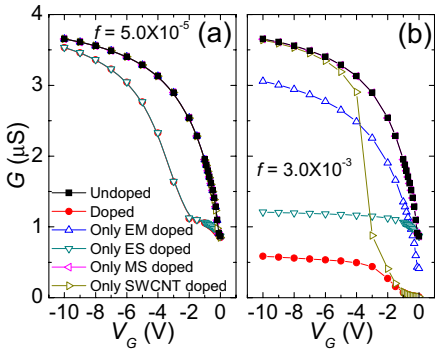

FIG. 3. (Color online) Conductance (hole) response to (a) low doping $f=5.0\times10^{-5}$/atom and (b) high doping $f=3.0\times10^{-3}$/atom for a specific CNNFET with $L_C=5$ μm and the nanotube density of 4 μm^{-2}. Also shown is the conductance response when only one kind of components (SWCNTs, EM contacts, ES contacts or MS junctions) is doped.

sitive to doping, they do little contribution to the conductance of CNNFETs due to their extremely low conductance and hence could not be responsible for the doping-induced conductance change either. As a result, the doping-induced conductance change in CNNFETs is determined by ES and EM contacts. This conclusion is supported by the simulation results for V_G-dependent hole conductance of a CNNFET in Fig. 3. Under doping, only ES and EM contacts have appreciable contributions to the conductance change. In particular, when approaching the detection limit of low doping [Fig. 3(a)], only ES contacts are responsible. In contrast, doping in SWCNTs contributes significantly only in high f and low V_G region [Fig. 3(b)], which suggests their negligible effects in low f and high V_G region, the preferred operation conditions for normal sensing. Interestingly, here comes an unexpected observation that even if the sensing mechanism of CNNFETs is dominated by electron doping instead of work-function modulation, the responsible region is actually near the electrode-SWCNT contacts, not in the channel region. Our simulation results show that electron doping can effectively reduce the electrode-SWCNT contact conductance [Figs. 2(e) and 4(a)] by thickening the barrier at the electrode-SWCNT interface [Fig. 4(b)]. Therefore, the conductance change of the electrode-SWCNT contacts should not always be ascribed to the work-function modulation of the electrode metal. It can also result from doping. In addition, doping is found to take effect only when the doping region is close to the electrode-SWCNT interface. Figure 4 also shows the conductance of the ES contacts with partially doped SWCNT, where there is an undoped region of width w at the electrode-SWCNT interface. When w is as wide as about 10 nm, the effects of doping disappear. It is clear in Fig. 4(b) that at ON state, the barrier at the ES contact is very thin (a few nm). Without doping in the barrier region, the barrier cannot be thickened so that no significant conductance change can be seen. Therefore, in order to achieve observable doping-induced electrical signal in CNNFETs, doping should take place very close to the electrode-SWCNT interface. This may provide an explanation to the experimental observations that showed no distinct electrical signal when the electrodes were passivated by photoresist[8] or chemicals.[9]

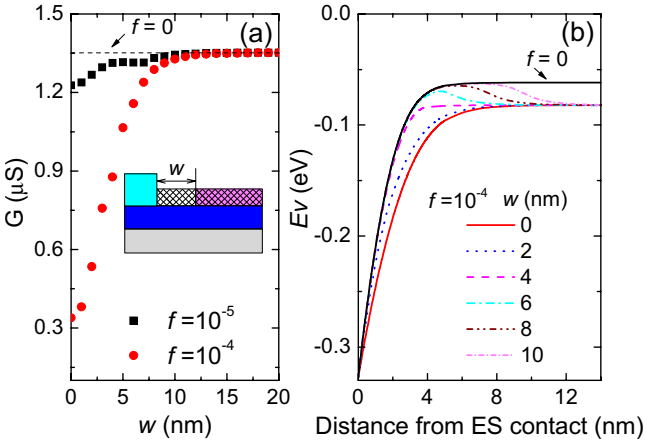

FIG. 4. (Color online) (a) The conductance ($V_G=-10$ V) response of ES contacts to partial doping of the s-SWCNT for $f=10^{-5}$ and 10^{-4}/atom, respectively. The inset shows the partially doped ES contacts, where w is the width of the undoped region at the electrode-SWCNT interface. (b) Valence band E_V diagram of undoped ($f=0$) and partially doped ($f=10^{-4}$/atom) ES contacts for different w. The energy is referenced to the Fermi level. $\Delta W=0$ eV.

B. Reduction in sensitivity

As demonstrated above, ES contacts are the predominant region of CNNFET-based sensors for detecting biomolecules in low-concentration analytes. Figure 5(a) shows the normalized conductance G/G_0 of the ES contact conductance at low doping, where G_0 is the conductance at $f=0$. The doping sensitivity of the ES contacts decreases with increasing ΔW, which can be readily understood. For low ΔW (i.e., high barrier to holes), the injected carriers from the electrodes are

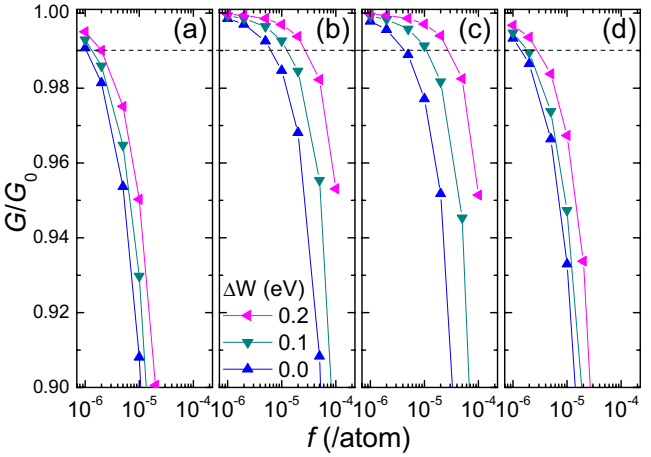

FIG. 5. (Color online) Simulated doping dependence of normalized conductance (G/G_0) at various ΔW for (a) ES contacts, (b) high-density CNNFETs (4 μm^{-2}), and (c) low-density CNNFETs (2 μm^{-2}) without any spanning metallic paths and (d) the same CNNFETs as (b) but here the SS junctions are assumed to have improved conductance of G_q. The dashed line shows that the conductance change is as significant as 1%. Each data point for CNNFETs is the average over the results of 200 independent simulation attempts.

less and the effects of doped carriers are more significant resulting in higher sensitivity. This is in agreement with the experimental results[8] where CNNFETs contacted with different electrode metals were found to have different sensitivities. In Fig. 5(a), when the doping approaches $f \approx 10^{-6}$/atom, easily detectable conductance changes (>1%) have already been seen. So far there seems no general formula relating the doping fraction f to the concentration C_0 of the detected biochemical analyte. However, one can roughly estimate the detection limit by the simple scaling relationship,[40]

$$Nf \approx 2\pi D C_0 t_s, \tag{8}$$

where t_s is the response or settling time to capture the biomolecules to reach a certain doping fraction f on SWCNTs and D is the diffusion coefficient of biomolecules. For protein or low-base-pair DNAs, D is usually around 10^{-6} cm^2/s,[40–42] and t_s is of the order of 100 s.[7,9,43] Hence, $f=10^{-6}$/atom ($d \sim 1.0$ nm) corresponds to $C_0 \approx 3$ fM. However, in practice, the detection limit of usual CNNFETs for proteins or DNAs is at the level of pM.[7] Consistently, our simulation results in Fig. 5(b) also show that compared with ES contacts, the G/G_0-f curves of CNNFETs diffuse in the direction of high doping, implying significantly reduced sensitivity, especially at high ΔW, corresponding to, e.g., Au,[44] the frequently used electrode metal in CNNFET-based sensors.

At first sight, the percolated m-SWCNT subnetworks would form high-conductance but insensitive metallic paths which might reduce the sensitivity of CNNFETs. However, at ON state, the s-SWCNT subnetworks in long-channel CNNFETs ($L_C > L_S$) have comparable conductance with the m-SWCNT subnetworks. The effect of metallic paths should not be significant as shown in Fig. 5(c), where the nanotube density is decreased to avoid percolated metallic paths, but the sensitivity is not conclusively improved.

Here we propose a more reasonable mechanism for the sensitivity reduction in CNNFETs. At ON state, the ES contact conductance may compare with that of SS junctions. With plenty of SS junctions in the nanotube networks, the conductance of CNNFETs is actually dominated by SS junctions. Since SS junctions are shown in Fig. 2(e) to be insensitive to doping, the sensitivity of CNNFETs is reduced as a result. The effect of SS junctions can be confirmed by the simulation results in Fig. 5(d), where the significance of SS junctions is suppressed by assuming their conductance to be as high as G_q and the sensitivity of CNNFETs improves obviously. When the ES contact conductance is improved, for example, by increasing ΔW (i.e., decreasing the barrier to holes), the effect of SS junctions should be more significant and hence the sensitivity would reduce more severely, as shown in Fig. 5(b).

C. Channel-length dependent sensitivity

Considering the significant effect of SS junctions on the sensitivity of CNNFETs, an alternative to improve the sensitivity is to use small L_C devices. Decreasing L_C leads to a decrease in the number of SS junctions and thus the sensitivity is increased. Previous experimental studies[8] have also suggested that shorter channel CNNFETs have higher sensitivity for DNA detection. Here, we have found that for different doping, CNNFETs have different scaling behaviors with respect to sensitivity. For low doping, due to the effects of SS junctions, the sensitivity increases with decreasing channel length L_C as expected (Region I in Fig. 6). For high doping, the conductance of ES contacts is completely suppressed by electron doping resulting in negligible conductance contribution of the s-SWCNT subnetworks. For such high doping, EM contacts are sensitive. Therefore, CNNFETs behave similarly to those at low doping except that the responsible part is the m-SWCNT subnetworks, not the s-SWCNT subnetworks. Therefore we can see in Region III of Fig. 6, like that at low doping, sensitivity also increases with decreasing L_C. However, here the scaling behavior of sensitivity is attributed to the effects of MM junctions, which act similarly to the SS junctions in low-doping CNNFETs.

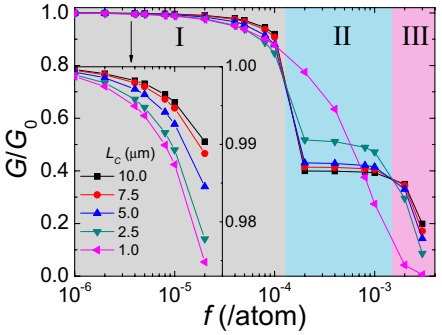

FIG. 6. (Color online) Doping dependence of normalized conductance of CNNFETs with different channel length. The nanotube density is 4 μm^{-2} and $\Delta W=0.1$ eV. Within Regions I, II, and III, long-channel devices exhibit identical scale behavior of sensitivity, respectively. Short-channel ($L_C=1.0$ μm) devices obey the same scaling rule almost throughout the doping region except those near the transition between the three regions. Each data point is the average over the results of 200 independent simulation attempts.

Interestingly, as shown in Region II of Fig. 6, different from low- and high-doping regions, in medium-doping region the sensitivity decreases with decreasing L_C. Note that at medium doping [i.e., around the marked region in Fig. 2(e)], the ES contact conductance is negligible and meanwhile the EM contacts are weakly sensitive to doping. Hence, neither SS nor MM junctions are responsible for the scaling behavior of sensitivity. Since in this case the doped conductance G is approximately the conductance of m-SWCNT subnetworks in undoped CNNFETs, the normalized conductance G/G_0 is nearly the conductance percentage of the m-SWCNT subnetworks in undoped CNNFETs. Because EM contacts have much higher conductance than ES contacts, with increasing the same number of MM/SS junctions, conductance reduction in the m-SWCNT subnetworks is more significant than that in the s-SWCNT subnetworks. Longer-channel CNNFETs have more intertube junctions and hence are of smaller conductance percentage of the m-SWCNT subnetworks. Therefore, longer-channel CNNFETs have smaller G/G_0, i.e., higher sensitivity.

Figure 7 exhibits the experimental[8] and simulated results of the channel-length effect on electrical sensing of DNA. In

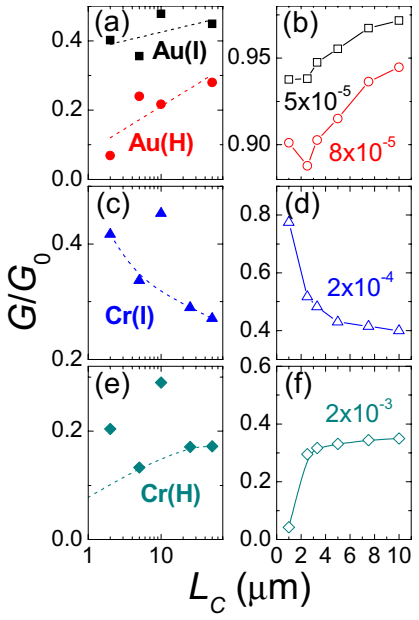

FIG. 7. (Color online) Comparison of experimental (data are from Table 2 in Ref. 8) and simulation results of the channel-length effects on the normalized conductance of CNNFETs. The experiments are for (a) Au-contacted CNNFETs upon immobilization [Au(I)] and hybridization [Au(H)], (c) Cr-contacted CNNFETs upon immobilization [Cr(I)], and (e) Cr-contacted CNNFETs upon hybridization [Cr(H)]. The dashed curves in (a), (c), and (e) are meant as guides to the eyes. The simulation is performed for CNNFETs ($4\ \mu m^{-2}$, $\Delta W=0.1$ eV) in (b) low-doping region, $f=5\times10^{-5}$ and 8×10^{-5}, (d) medium-doping region, $f=2\times10^{-4}$ and (f) high-doping region $f=2\times10^{-3}$. $L_S=2\ \mu m$ for simulations and $L_S=5\sim10\ \mu m$ for experiments. Each simulation data point is the average over the results of 200 independent simulation attempts.

Ref. 8, the conductance response of biosensors based on Au-contacted and Cr-contacted CNNFETs is carefully studied. According to our analysis above, these sensors most likely worked in different doping regions. The Au-contacted CNNFETs would work in the low-doping region since after either immobilization or hybridization, the ON-state ($V_G=-10$ V) conductance was higher than the OFF-state ($V_G=10$ V) conductance of the bare (undoped) devices [see Fig. 3(a) in Ref. 8], implying that the conductance of the s-SWCNT subnetworks was not completely suppressed. For the Cr-contacted CNNFETs after immobilization, they should work in the high-doping region since the ON-state conductance was lower than the OFF-state conductance of the bare devices [see Fig. 3(b) in Ref. 8], suggesting an appreciable sensitivity of the m-SWCNT subnetworks. After hybridization, they should work in the medium-doping region since the ON-state conductance was close to the OFF-state conductance of the bare devices [see Fig. 3(b) in Ref. 8], indicating a complete suppression of the s-SWCNT subnetworks and weak sensitivity of the m-SWCNT subnetworks. According to the classification of doping regions here, consistency in the scaling behavior of sensitivity is evidently shown in Fig. 7 between the simulation and experimental results. Note that in Ref. 8, the Cr-contacted CNNFETs show exceptional conductance reduction upon immobilization. After hybridization, the conductance increases unexpectedly. Our analysis is in agreement with Ref. 8 in that electronic doping is not the only major contributing factor for DNA sensing in this case. A possible explanation to the electrical behavior is that the process of immobilization has not only introduced electron doping, but also modulated the electrode work function probably through interaction between Cr and DNAs. Consequently, an extremely low conductance was obtained. The process of hybridization recovered to some extent the effect of the Cr-DNA interaction and hence only doping was responsible so that the conductance increased though the CNNFETs should be more heavily doped after hybridization. However, no matter whether doping or work-function modulation is responsible, they can only effectively influence the conductance of the ES or EM contacts. In this sense, work-function modulation can be regarded as extra doping. Therefore, after immobilization the sensitivity of the Cr-contacted CNNFETs exhibited the scaling behavior in the high-doping region though the actual doping might not be really so high.

Short-channel devices ($L_C<L_S$) seem to be the preferable alternative as it comes to improvement of the detection limit for CNNFET-based biosensors since they can completely avoid the negative effects of the SS junctions and thus improve the sensitivity at low-doping levels. However, in short-channel devices, metallic paths may have significantly higher conductance than the s-SWCNT subnetworks due to the lack of MM junctions. In this case, the effect of metallic paths, high conductance but insensitive, may become prominent and the sensitivity of CNNFETs can also decrease [Fig. 7(b)]. The significant effects of metallic paths in short-channel devices can also be confirmed in Fig. 6, where around the two boundaries of Region II, which is dominated by the conductance percentage of metallic paths, the short-channel devices ($L_C=1.0\ \mu m$) exhibit unexpected scaling behaviors in contrast to long-channel devices.

IV. CONCLUSIONS

In conclusion, systematic theoretical studies have been performed to investigate the essence of doping-dominated sensing of biomolecules using CNNFETs. The simulation shows that the contribution of the SWCNTs to the doping-induced ON-state conductance change is negligible due to their invisible effect on the conductance of CNNFETs and insensitivity to doping whereas the contribution of electrode-SWCNT contacts is significant. If the doping region covers the close vicinity of the electrode-SWCNT interfaces, the interface barrier thickness can be effectively altered resulting in significant conductance change in the electrode-SWCNT contacts. Therefore similar to work-function modulations, the responsible part for the doping-dominated conductance change in CNNFET-based biosensors is also the electrode-SWCNT contacts. It is not the channels themselves, in contrast to previous assumptions. However, for long-channel devices, the insensitive SS and MM junctions in the channel may significantly reduce the sensitivity of CNNFETs. These intertube junctions should also be responsible for the scaling behavior of sensitivity found experimentally. Our systematic simulation shows that the sensitivity increases with decreas-

ing channel length in low and high-doping regions due to the effects of SS and MM junctions, respectively, while decreases in medium-doping region due to the effects of the conductance percentage of metallic paths. In low-doping region, the effects of metallic paths are negligible for long-channel devices. Nevertheless, for short-channel devices such effects might become prominent possibly also resulting in reduced sensitivity. In order to improve the detection limit of CNNFET-based biosensors, the effects of both intertube junctions and metallic paths should be suppressed appropriately.

ACKNOWLEDGMENTS

This work was financially supported by Swedish Research Council (VR) (Grant No. 621-2005-5971) and Swedish Agency for Innovation Systems (VINNOVA) (Grant No. 2005-01138).

*Corresponding author; shili@kth.se

[1] E. S. Snow, J. P. Novak, P. M. Campbell, and D. Park, Appl. Phys. Lett. **82**, 2145 (2003).
[2] Q. Cao, H.-S. Kim, N. Pimparkar, J. P. Kulkarni, C. Wang, M. Shim, K. Roy, M. A. Alam, and J. A. Rogers, Nature (London) **454**, 495 (2008).
[3] M. C. LeMieux, M. Roberts, S. Barman, Y. W. Jin, J. M. Kim, and Z. Bao, Science **321**, 101 (2008).
[4] C. Kocabas, N. Pimparkar, O. Yesilyurt, S. J. Kang, M. A. Alam, and J. A. Rogers, Nano Lett. **7**, 1195 (2007).
[5] E. S. Snow, F. K. Perkins, and J. A. Robinson, Chem. Soc. Rev. **35**, 790 (2006).
[6] A. Star, E. Tu, J. Niemann, J.-C. P. Gabriel, C. S. Joiner, and C. Valcke, Proc. Natl. Acad. Sci. U.S.A. **103**, 921 (2006).
[7] H. R. Byon and H. C. Choi, J. Am. Chem. Soc. **128**, 2188 (2006).
[8] E. L. Gui, L.-J. Li, K. Zhang, Y. Xu, X. Dong, X. Ho, P. S. Lee, J. Kasim, Z. X. Shen, J. A. Rogers, and S. G. Mhaisalkar, J. Am. Chem. Soc. **129**, 14427 (2007).
[9] R. J. Chen, H. C. Choi, S. Bangsaruntip, E. Yenilmez, X. Tang, Q. Wang, Y.-L. Chang, and H. Dai, J. Am. Chem. Soc. **126**, 1563 (2004).
[10] K. Bradley, M. Briman, A. Star, and G. GrUner, Nano Lett. **4**, 253 (2004).
[11] X. Tang, S. Bansaruntip, N. Nakayama, E. Yenilmez, Y.-L. Chang, and Q. Wang, Nano Lett. **6**, 1632 (2006).
[12] A. Star, J.-C. P. Gabriel, K. Bradley, and G. GrUner, Nano Lett. **3**, 459 (2003).
[13] S. Kumar, J. Y. Murthy, and M. A. Alam, Phys. Rev. Lett. **95**, 066802 (2005).
[14] M. A. Alam, N. Pimparkar, S. Kumar, and J. Murthy, MRS Bull. **31**, 466 (2006).
[15] A. Behnam and A. Ural, Phys. Rev. B **75**, 125432 (2007).
[16] J. Li, Z.-B. Zhang, and S.-L. Zhang, Appl. Phys. Lett. **91**, 253127 (2007).
[17] J. Li, Z.-B. Zhang, M. Östling, and S.-L. Zhang, Appl. Phys. Lett. **92**, 133103 (2008).
[18] S. Kumar, N. Pimparkar, J. Y. Murthy, and M. A. Alam, Appl. Phys. Lett. **88**, 123505 (2006).
[19] N. Pimparkar, Q. Cao, S. Kumar, J. Y. Murthy, J. Rogers, and M. A. Alam, IEEE Electron Device Lett. **28**, 157 (2007).
[20] J. Guo, S. Goasguen, M. Lundstrom, and S. Datta, Appl. Phys. Lett. **81**, 1486 (2002).
[21] J. W. Mintmire and C. T. White, Phys. Rev. Lett. **81**, 2506 (1998).
[22] J.-C. Charlier, X. Blase, and S. Roche, Rev. Mod. Phys. **79**, 677 (2007).
[23] F. Léonard and J. Tersoff, Phys. Rev. Lett. **83**, 5174 (1999).
[24] F. Léonard and J. Tersoff, Phys. Rev. Lett. **84**, 4693 (2000).
[25] A. A. Odintsov, Phys. Rev. Lett. **85**, 150 (2000).
[26] A. A. Odintsov and Y. Tokura, J. Low Temp. Phys. **118**, 509 (2000).
[27] O. Wunnicke, Appl. Phys. Lett. **89**, 083102 (2006).
[28] Y.-F. Chen and M. S. Fuhrer, Phys. Rev. Lett. **95**, 236803 (2005).
[29] V. Perebeinos, J. Tersoff, and Ph. Avouris, Nano Lett. **6**, 205 (2006).
[30] K. K. Young, IEEE Trans. Electron Devices **36**, 399 (1989).
[31] F. G. Pikus and K. K. Likharev, Appl. Phys. Lett. **71**, 3661 (1997).
[32] J. Appenzeller, M. Radosavljevic, J. Knoch, and P. Avouris, Phys. Rev. Lett. **92**, 048301 (2004).
[33] T. Nakanishi, A. Bachtold, and C. Dekker, Phys. Rev. B **66**, 073307 (2002).
[34] F. Léonard and A. A. Talin, Phys. Rev. Lett. **97**, 026804 (2006).
[35] S. Heinze, M. Radosavljevic, J. Tersoff, and P. Avouris, Phys. Rev. B **68**, 235418 (2003).
[36] M. S. Fuhrer, J. Nygård, L. Shih, M. Forero, Y.-G. Yoon, M. S. C. Mazzoni, H. J. Choi, J. Ihm, S. G. Louie, A. Zettl, and P. L. McEuen, Science **288**, 494 (2000).
[37] J. Tersoff, Appl. Phys. Lett. **74**, 2122 (1999).
[38] A. N. Andriotis, M. Menon, and G. E. Froudakis, Appl. Phys. Lett. **76**, 3890 (2000).
[39] E. S. Snow, J. P. Novak, M. D. Lay, and F. K. Perkins, Appl. Phys. Lett. **85**, 4172 (2004).
[40] P. R. Nair and M. A. Alam, Appl. Phys. Lett. **88**, 233120 (2006).
[41] D. Brune and S. Kim, Proc. Natl. Acad. Sci. U.S.A. **90**, 3835 (1993).
[42] M.-K. Liu, P. Li, and J. C. Giddings, Protein Sci. **2**, 1520 (1993).
[43] C. Li, M. Curreli, H. Lin, B. Lei, F. N. Ishikawa, R. Datar, R. J. Cote, M. E. Thompson, and C. Zhou, J. Am. Chem. Soc. **127**, 12484 (2005).
[44] X. Cui, M. Freitag, R. Martel, L. Brus, and Ph. Avouris, Nano Lett. **3**, 783 (2003).